PAPER

Check for updates

Quantum chemical modification of indaceno dithiophene-based small acceptor molecules with enhanced photovoltaic aspects for highly efficient organic solar cells†

Ehsan Ullah Rashid,[a] N. M. A. Hadia, [ID] *[b] Omaymah Alaysuy,[c] Javed Iqbal, [ID] *[ag] M. M. Hessien,[d] Gaber A. M. Mersal,[d] Rana Farhat Mehmood,[e] Ahmed M. Shawky, [ID] [f] Muhammad Imran Khan[a] and Rasheed Ahmad Khera [ID] *[a]

In this computational work, with the aim of boosting the ultimate efficiency of organic photovoltaic cells, seven small acceptors (IDST1–IDST7) were proposed by altering the terminal-acceptors of reference molecule IDSTR. The optoelectronic characteristics of the IDSTR and IDST1–IDST7 molecules were investigated using the MPW1PW91/6-31G(d,p) level of theory, and solvent-state computations were examined using time-dependent density functional theory (TD-DFT) simulation. Nearly all the investigated photovoltaic aspects of the newly proposed molecules were found to be better than those of the IDSTR molecule *e.g.* in comparison to IDSTR, IDST1–IDST7 exhibit a narrower bandgap (E_{gap}), lower first excitation energy (E_x), and a significant red-shift in the absorbance maxima (λ_{max}). According to the findings, IDST3 has the lowest E_x (1.61 eV), the greatest λ_{max} (770 nm), and the shortest E_{gap} (2.09 eV). IDST1–IDST7 molecules have higher electron mobility because their RE of electrons is less than that of IDSTR. Hole mobility of IDST2–IDST7 is higher than that of the reference owing to their lower RE for hole mobility than IDSTR. By coupling with the PTB7-Th donor, the open circuit voltage (V_{OC}) of the investigated acceptor molecules (IDSTR and IDST1–IDST7) was calculated and investigation revealed that IDST4–IDST6 molecules showed higher V_{OC} and fill factor (FF) values than IDSTR molecules. Accordingly, the modified molecules can be seriously evaluated for actual use in the fabrication of OSCs with enhanced photovoltaic and optoelectronic characteristics in light of the findings of this study.

1 Introduction

A lot of work in the areas of novel material research and device technology has led to significant breakthroughs in organic solar cells (OSCs).[1,2] Different active layer materials, color customization, being light-weight, their transparency, and their

[a]*Department of Chemistry, University of Agriculture, Faisalabad 38000, Pakistan. E-mail: javedkhattak79@gmail.com; javed.iqbal@uaf.edu.pk; rasheedahmadkhera@ yahoo.com; rasheed.ahmad.khera@uaf.edu.pk*

[b]*Physics Department, College of Science, Jouf University, P.O. Box 2014, Sakaka, Al-Jouf, Saudi Arabia. E-mail: nmhadia@ju.edu.sa*

[c]*Department of Chemistry, College of Science, University of Tabuk, 71474, Tabuk, Saudi Arabia*

[d]*Department of Chemistry, College of Science, Taif University, P.O. Box 11099, Taif, 21944, Saudi Arabia*

[e]*Department of Chemistry, Division of Science and Technology, University of Education, Township, Lahore 54770, Pakistan*

[f]*Science and Technology Unit (STU), Umm Al-Qura University, Makkah 21955, Saudi Arabia*

[g]*Department of Chemistry, College of Science, University of Bahrain Zallaq, Bahrain*

† Electronic supplementary information (ESI) available. See https://doi.org/10.1039/d2ra05239c

flexibility are just a few of the many benefits of OSCs over silicon solar cells. Attributed to these benefits, OSCs are now considered among the technologies with the most potential for converting solar energy. The donor–acceptor mix in the photo-active layer influences the device performance of OSCs that are bulk heterojunction (BHJ) types.[3,4] Fullerene acceptors (FAs) encounter a few significant issues that hinder the device's performance from improving any further: problems with chemical alteration, limited energy level tenability,[5] structural instability as well as non-significant UV-visible and near-infrared (NIR) absorption.[6,7] Non-fullerene acceptors (NFAs) offer a greater capacity to address these issues than FAs.[1,8,9] With comprehensive spectrum coverage, great synthesizing adaptability, minimal voltage loss, and adjustable optoelectronic aspects, NFAs were able to achieve power conversion efficiency (PCE) of over 17%.[10–14]

It is widely acknowledged that a deeper comprehension of the link between structure and performance is necessary to boost PCEs and the ultimate growth of OSCs. This is due to the fact that slight changes in molecular structures frequently lead to different BHJ variations, including changes in molecular configurations and van der Waals interactions. These variations may have

complex effects on exciton/charge behaviors as well as general efficiencies. In order to get a more comprehensive understanding of designing proficient OSCs, a thorough structural modification of small molecule acceptors (SMAs) is still greatly sought.

Several investigations have shown that decreasing the bandgap (E_{gap}) may be achieved by enhancing the electron donating capacity of the donor component by expanding the efficient conjugate part.[15] One simple way to accomplish this objective is to extend the core by increasing the fused-rings to extend conjugation in the core that is the donor part of molecule.[16,17] However, this method didn't extend the spectrum of absorbance as anticipated, and flaws were found, including low solubility and time-consuming synthesis and purifying stages.[18] On the other hand, these issues may be avoided by including heteroatom-based π-bridges into the conjugate system in order to lengthen it through non-covalent forces present within a molecule.[19–21]

Polymeric donor and NFAs photovoltaic compounds have benefited from the promising consideration of the asymmetric technique.[22–24] Consequently, several studies have been reported that include the addition of π-bridges in the molecules in an asymmetric way.[25,26] Recent research introduced a single bridge of alkythio-linked thiophene into an extremely crystalline indaceno dithiophene based small molecule (ID-4F). The conjugation was increased and the NFA's E_{gap} was dramatically decreased because of the non-covalent forces (oxygen–sulfur and sulfur–sulfur) and ability to donate electrons in a significant way *via* these π-bridges. High energy levels and a redshift in the absorption spectrum, improved short circuit current (J_{SC}) as well as 14.3% PCE of the resultant acceptor molecule (IDST-4F) were achieved.[25]

In the present investigation, indaceno dithiophene and alkythio-linked thiophene bridge-based molecule (IDST-4F) is used as the reference molecule (**IDSTR**), with the exception that the alkyl side chains have been swapped out with simple methyl groups to save computational costs. The donor core of **IDSTR** molecule is consist of 4,4,9,9-tetramethyl-4,9-dihydro-*s*-indaceno[1,2-*b*:5,6-*b'*]dithiophene and 3-methylsulfanyl-thiophene bridge is present on one side of the core of molecule making overall an asymmetric geometry of molecule. In this research, we have regarded both indaceno dithiophene and methylsulfanyl-thiophene units as the donor component of the molecule, as the scientists who designed the bridge that was added to the ID-4F molecule to boost the electron-donating function of the donor core unit. The donor portion of **IDSTR** is further attached to the molecules' ends by 2-(5,6-difluoro-2-methylene-3-oxo-indan-1-ylidene)-malononitrile units, forming an acceptor–donor–acceptor (A–D–A) type molecule. We have proposed seven new acceptor molecules (**IDST1–IDST7**) by swapping out the ending acceptor component of the **IDSTR** molecule with seven different acceptor groups. 1-Dicyanomethylene-6-methyl-2-methylene-3-oxo-indan-5-carboxylic acid methyl ester; compound with methanedione (**IDST1**), 6-cyano-1-dicyanomethylene-2-methylene-3-oxo-indan-5-carboxylic acid methyl ester (**IDST2**), 1-dicyanomethylene-2-methylene-3-oxo-indan-5,6-dicarbonitrile (**IDST3**), 2-(2-methylene-3-oxo-2,3-dihydro-cyclopenta[*b*]naphthalen-1-ylidene)-malononitrile (**IDST4**), 2-(2-bromo-6-methylene-7-oxo-6,7-

dihydro-1-thia-*s*-indacen-5-ylidene)-malononitrile (**IDST5**), 2-(6,7-difluoro-2-methylene-3-oxo-2,3-dihydro-cyclopenta[*b*]naphthalen-1-ylidene)-malononitrile (**IDST6**) and 2-(1-chloro-6-oxo-5,6-dihydro-cyclopenta[*c*]thiophen-4-ylidene)-malononitrile (**IDST7**) are the new acceptor groups of **IDST1–IDST7** molecules respectively as shown in Fig. 1.

2 Computational approaches

All molecular geometry calculations were done in Gaussian 09,[27] and 3D molecular structures were modelled and viewed in GaussView 6.0.16.[28] To aid the optimization of the **IDSTR**, DFT calculations were performed using the B3LYP,[29] CAM-B3LYP,[30] MPW1PW91,[31] and ωB97XD[32] functionals in conjunction with the 6-31G(d,p) basis set. Time-dependent density functional theory (TD-DFT)[33] computations were employed to forecast **IDSTR** UV-visible absorption properties after the optimization of geometries and Integral Equation Formalism Polarizable Continuum Model (IEFPCM) model[34] was for the investigation of the effect of solvent (chloroform).

To verify the feasibility of the theoretical approach, the maximum absorption (λ_{max}) of **IDSTR** from four above mentioned functionals was verified with the experimental λ_{max} provided in the literature. When comparing the practical λ_{max} of **IDSTR** (728 nm)[25] to the four computed absorption values *i.e.* 757 nm, 536 nm, 712 nm and 513 nm correspondingly, we found that the modified Perdew–Wang 1-parameter (MPW1PW91) functional was the closest to the empirical value[25] indicating that the combination of this level of theory will be best for computing proposed molecules, as shown in Table 1.

The molecules' UV-visible spectra were generated with the help of Origin 6.0.[35] Transition density matrix (TDM) measurements were transformed into visualizations of movement and interaction of excitons using Multiwfn software.[36] PyMOlyze 1.1 (ref. 37) was employed to create the density of states (DOS) graphs.[38] Marcus theory can be used to examine the extent of charge mobility, both intermolecularly and intramolecularly, by analyzing the reorganization energy (RE).[39,40] Recent efforts of ours, however, have centred on the intramolecular charge transfer (ICT). RE is the sum of two reorganizational forces, one external and one internal. Rapid fluctuations in the outer environment and polarisation alterations during charge transport are in external RE,[41] whereas the internal RE mainly depends on molecular structural variation. External RE cannot support our calculations, hence for the sake of our research, we only concentrate on internal RE. Using the given eqn (1) and (2), the RE for the mobility of hole (λ_+) and electron (λ_-) was calculated.

$$\lambda_+ = [E_+^0 - E_0] + [E_0^+ - E_+] \tag{1}$$

$$\lambda_- = [E_-^0 - E_0] + [E_0^- - E_-] \tag{2}$$

E_0^+ and E_0^- are the cation and anion ground state energies calculated from ground state optimized neutral molecule. E_+ and E_- are the energies of cation and anion computed from cation and anion optimized models. E_+^0 and E_-^0 and are the
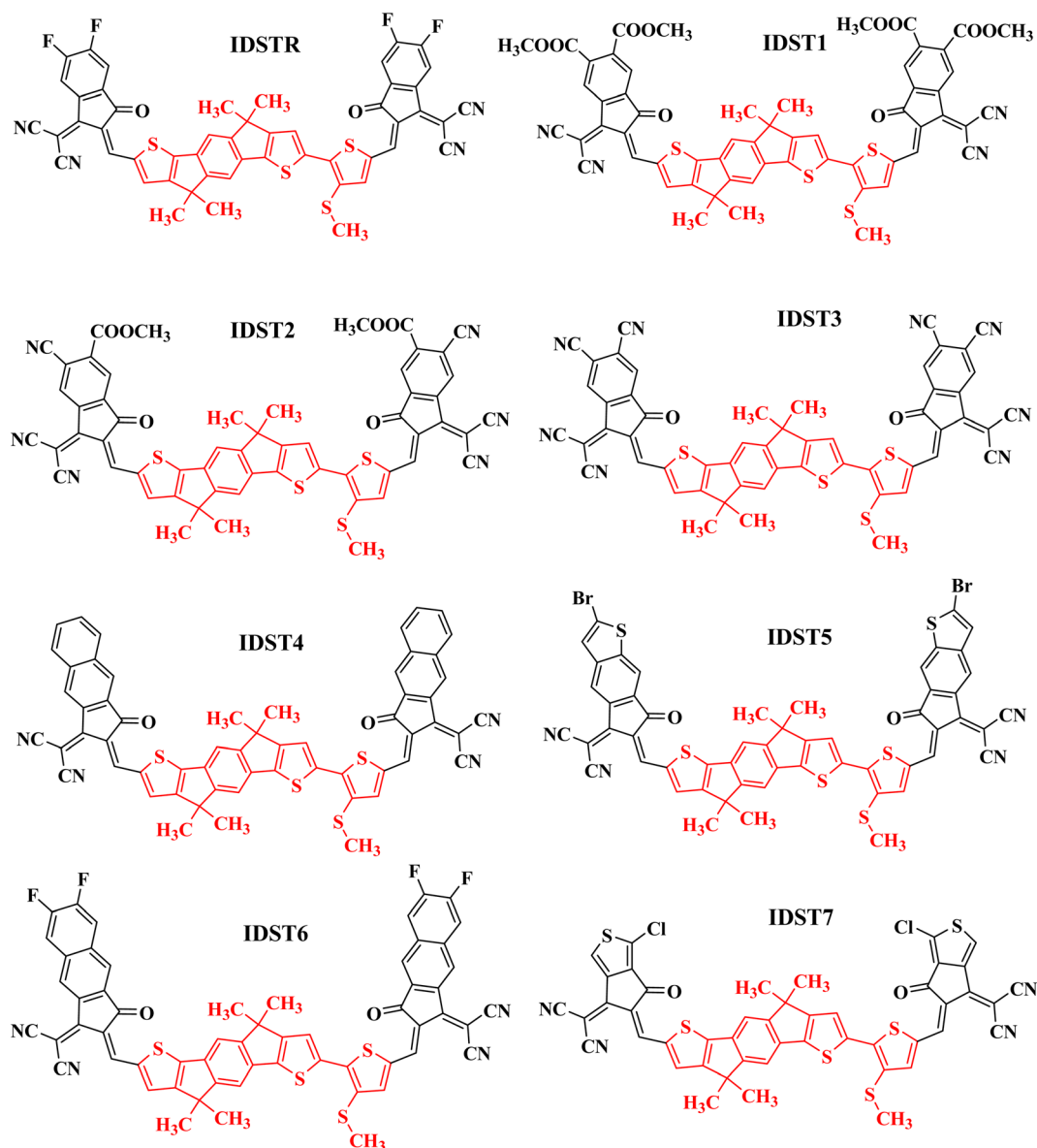
Fig. 1 ChemDraw structures of **IDSTR** and **IDST1–IDST7** molecules, the red part indicating the donor and black part indicating acceptor site of the molecule.

Table 1 Maximum absorption of **IDSTR** using four different functionals and experimental λ_{max} of **IDSTR**

Molecule	B3LYP	CAM-B3LYP	MPW1PW91	wB97XD	Exp. λ_{max}
IDSTR	757 nm	536 nm	712 nm	513 nm	728 nm

neutral molecules' energies, that are calculated utilizing optimized cation and anion geometries. E_0 is the ground state energy of molecule neutrally optimized.[42]

3 Results and discussion

3.1. Structural optimization

Optoelectronic characteristics are strongly influenced by molecular structure.[43] The reference molecule (**IDSTR**) and the recently proposed molecules (**IDST1–IDST7**) have been optimized using the DFT functional that was picked as the best fit as represented in Fig. 2. An effective charge transfer is possible due to the molecules' extended conjugation, which extends from the center to the ending regions of the molecule showing that charge transport in these structures is robust due to the π-electrons delocalization. The dihedral angles ($\theta°$) and the bond length (L_b) were calculated to evaluate the level of conjugation as well as planarity of **IDSTR** and **IDST1–IDST7** molecules (Table 2). Double and single carbon bonds (C=C and C–C) have lengths of 1.34 Å and 1.54 Å, respectively. All the compounds investigated (**IDSTR** and **IDST1–IDST7**) had a L_b of around 1.41 Å, it demonstrates increased charge-transfer properties and permits the conjugation-mediated delocalization of π-electrons. All of the molecules that were investigated have $\theta°$ that
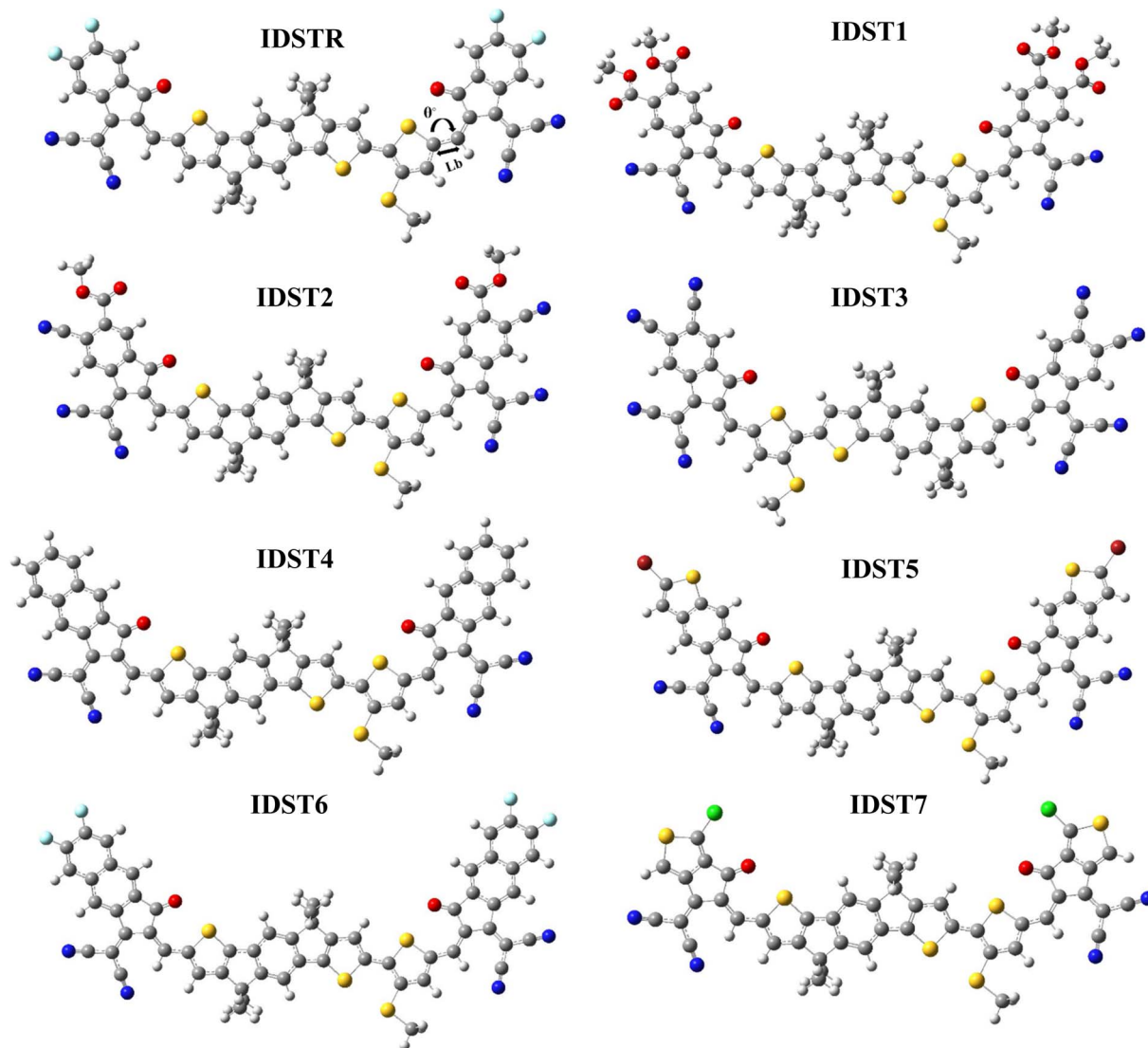
Fig. 2 Optimized structures of IDSTR and IDST1–IDST7 molecules.

fall within the range of 0.480°–0.669°. This indicates that all of the molecules have a planar geometry, as there is no twist in between end-capped acceptor and donor core, and there are also no groups that cause a hindrance.

Table 2 Computationally estimated L_b and dihedral angles ($\theta°$) of IDSTR and IDST1–IDST7 molecules

Molecules	L_b (Å)	$\theta°$
IDSTR	1.41	0.620
IDST1	1.41	0.480
IDST2	1.41	0.644
IDST3	1.41	0.607
IDST4	1.41	0.584
IDST5	1.41	0.669
IDST6	1.41	0.618
IDST7	1.41	0.015

3.2. Frontier molecular orbitals (FMOs) evaluation

Analysis of the FMOs is an essential scientific aspect for determining how well molecules facilitate charge movement and dispersion of electron density.[40] It is also useful in understanding the dispersion of charge facilitation and transmission in OSCs. Excitation takes place and electrons transmit from the valence to the conduction band.[73] The transmission of charges, light absorption, and electronic characteristics of chromophores are significantly influenced by their HOMO and LUMO energy. OSCs as well as other photovoltaic systems can be identified by the energy gap (E_{gap}), which demonstrates the necessity of exciton dissociation.[44] A smaller bandgap is indicative of a higher performing OSCs. Building functional PV devices requires the use of molecules with the lowest possible E_{gap}. Strong polarizability, poor kinetic stability, as well as great chemical reactivity are all characteristics of molecules with small E_{gap}.[45] Energy levels of HOMO, LUMO for **IDSTR** and

Table 3 HOMO and LUMO energies, E_{gap}, ionization potential (IP) and electron affinity (EA) of IDSTR and IDST1–IDST7 molecules

Molecules	HOMO (eV)	LUMO (eV)	E_{gap} (eV)	IP (eV)	EA (eV)
IDSTR	−5.75	−3.53	2.22	6.39	2.89
IDST1	−5.72	−3.53	2.19	6.34	2.92
IDST2	−5.90	−3.78	2.12	6.52	3.15
IDST3	−6.12	−4.03	2.09	6.85	3.33
IDST4	−5.59	−3.40	2.19	6.20	2.78
IDST5	−5.64	−3.43	2.21	6.25	2.83
IDST6	−5.69	−3.52	2.16	6.30	2.91
IDST7	−5.73	−3.54	2.19	6.36	2.91

IDST1–IDST7 HOMO as well as their E_{gap} are examined at select functionals to evaluate the influence of various end group acceptors on the photophysical characteristics of the analyzed molecules and their numerical data are shown in Table 3.

Fig. 3 displays HOMO and LUMO of every molecule under research with its corresponding E_{gap}. In the ground state, the majority of the charge is located on the center region of the molecule, which is the donor section. However, in the LUMO state, the charge potential shifts to the molecules' acceptor sites, which are located at their peripheral ends. It has been shown that the methylsulfanyl-thiophene bridge enhances the efficiency of charge transfer from the electron donating core to the electron pulling acceptors at that particular location. This strategy indicates the sequential charge transfer competencies

of donor core to the acceptor part from HOMO to LUMO. Furthermore, the efficient conjugation that is enabling the effective charge transfer capabilities owing to the planarity of the molecular geometries is shown by the charge transfer from the electron-rich donor portion to the acceptor part of the compound in the excited state. The **IDSTR** molecule's FMOs; HOMO and LUMO energies were measured to be −5.75 eV and −3.53 eV, respectively, and this molecule had a E_{gap} of 2.22 eV, which is higher than any of our recently proposed compounds. The **IDST3** molecule had the least HOMO energy (−6.12 eV) of any of the others, indicating that its HOMO is the stable of all the compounds under study. These **IDST3** molecules may be more stable because they have pairs of highly electronegative cyano groups in their peripheral acceptor units that has participated considerably in the charge density dispersal. Moreover, **IDST2** possesses the next most stable HOMO after **IDST3**, due to its comparatively low HOMO energy of −5.90 eV. The existence of both cyano and ester groups in the terminal sites of the **IDST2** molecule contributes to its stability. The decreasing patters of HOMO and LUMO energies for **IDSTR** and **IDST1–IDST7** molecules is IDST4 > IDST5 > IDST6 > IDST1 > IDST7 > IDSTR > IDST2 > IDST3 and IDST4 > IDST5 > IDST6 > IDST1 = IDSTR > IDST7 > IDST2 > IDST3 respectively. **IDST1–IDST7** molecules have smaller E_{gap} than **IDSTR**. The E_{gap} of the **IDST3** and **IDST2** is the smallest and second-smallest among all other recently proposed molecules, respectively, because of their strong peripheral acceptor site, which has contributed
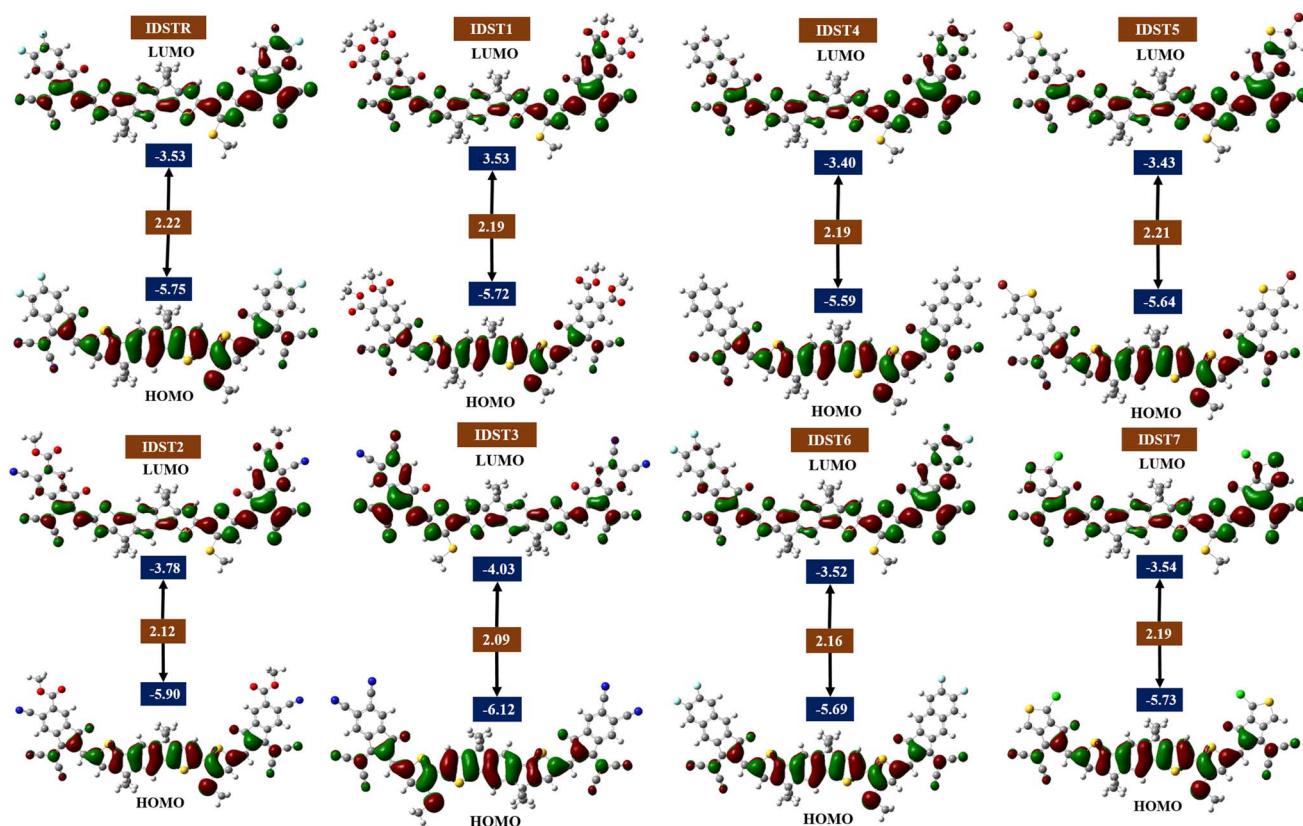

Fig. 3 FMOs of IDSTR and IDST1–IDST7 molecules.

sufficiently to improve molecules' ability to transfer charges and resultantly the bandgap is decreased. The descending trend of E_{gap} for studied molecules is **IDSTR > IDST5 > IDST1 = IDST4 = IDST7 > IDST6 > IDST2 > IDST3**.

3.3. Ionization potential and electron affinity

A number of variables, including IP and EA, can influence illustrate charge transfer efficacy. Energy released during an electron addition to a molecule is denoted as EA, whereas the energy input necessary for the donating an electron is indicated by IP.[46] Molecules with high IPs and EAs have stable HOMO energy states, making it more difficult to remove electrons, while those with low IPs and EAs have the capacity to release electron efficiently. The stabilization of the HOMO *via* electron withdrawing moieties is the cause of molecules with high IP and EA, while the destabilization of the HOMO by electron donating groups is the cause of molecules with low IP and EA.[47] In the current study, IP and EA were calculated using eqn (3) and (4).[48]

$$IP = [E_0^+ - E_0] \qquad (3)$$

$$EA = [E_0 - E_0^-] \qquad (4)$$

Table 3 contains the IP and EA estimates for the compounds **IDSTR** and **IDST1–IDST7**. The HOMO (−5.59 eV) of **IDST4** is the most destabilized among all hence possesses smallest IP (6.20 eV). **IDST4**, with a stabilized HOMO (−6.12 eV), has the highest EA (3.33 eV). Because **IDST5** has the second-least stable HOMO (−5.64 eV), it has the second-lowest IP (6.25 eV). **IDST2** has the second most stable HOMO (−5.90 eV), which contributes to its second greatest EA (3.15 eV).

3.4. Absorption spectrum

Quantum absorption spectra can be used to make reasonable estimate of the electrical specifications of chromophores. Tables 4 and 5 show the predicted results for the optical analysis of **IDSTR** and **IDST1–IDST7** molecules in the studied gaseous and solvent (chloroform) phases, respectively, of using MPW1PW91/6-31G(d,p) level of theory. The range of absorption spectrum for all investigated compounds (**IDSTR** and **IDST1–IDST7**) in gas phase is from around 350–1200 nm and in chloroform (CHCl$_3$) solvent is from around 350 to 1400 nm as shown

Table 4 Computed λ_{max}, excitation energy (E_x), oscillator strength (f) and assignment of IDSTR and IDST1–IDST7 molecules in gaseous phase

Molecules	Computed λ_{max} (nm)	E_x (eV)	f	Assignment
IDSTR	659	1.88	2.34	H–L (+98%)
IDST1	672	1.84	2.37	H–L (+99%)
IDST2	690	1.79	2.30	H–L (+99%)
IDST3	701	1.76	2.25	H–L (+98%)
IDST4	672	1.84	2.53	H–L (+99%)
IDST5	666	1.86	2.59	H–L (+98%)
IDST6	678	1.82	2.54	H–L (+98%)
IDST7	670	1.85	2.43	H–L (+97%)

Table 5 Computed λ_{max}, excitation energy (E_x), oscillator strength (f) and assignment of IDSTR and IDST1–IDST7 molecules in CHCl$_3$ solvent

Molecules	Exp. λ_{max} (nm)	Computed λ_{max} (nm)	E_x (eV)	f	Assignment
IDSTR	~728	712	1.74	2.58	H–L (+98%)
IDST1	—	732	1.69	2.57	H–L (+99%)
IDST2	—	753	1.65	2.50	H–L (+98%)
IDST3	—	770	1.61	2.42	H–L (+97%)
IDST4	—	724	1.71	2.78	H–L (+99%)
IDST5	—	717	1.73	2.81	H–L (+99%)
IDST6	—	731	1.70	2.79	H–L (+98%)
IDST7	—	723	1.71	2.71	H–L (+98%)

in Fig. 4. The λ_{max} of **IDSTR** in the former phase is 659 nm whereas its λ_{max} in CHCl$_3$ solvent is 712 nm. **IDST1–IDST7** molecules have a redshift in their λ_{max} compared to **IDSTR** in both the gas phase and the CHCl$_3$ solvent, with a range of 666–701 nm and 717–770 nm, respectively. Their UV-visible spectra show that all of the modified molecules exhibited a red shift
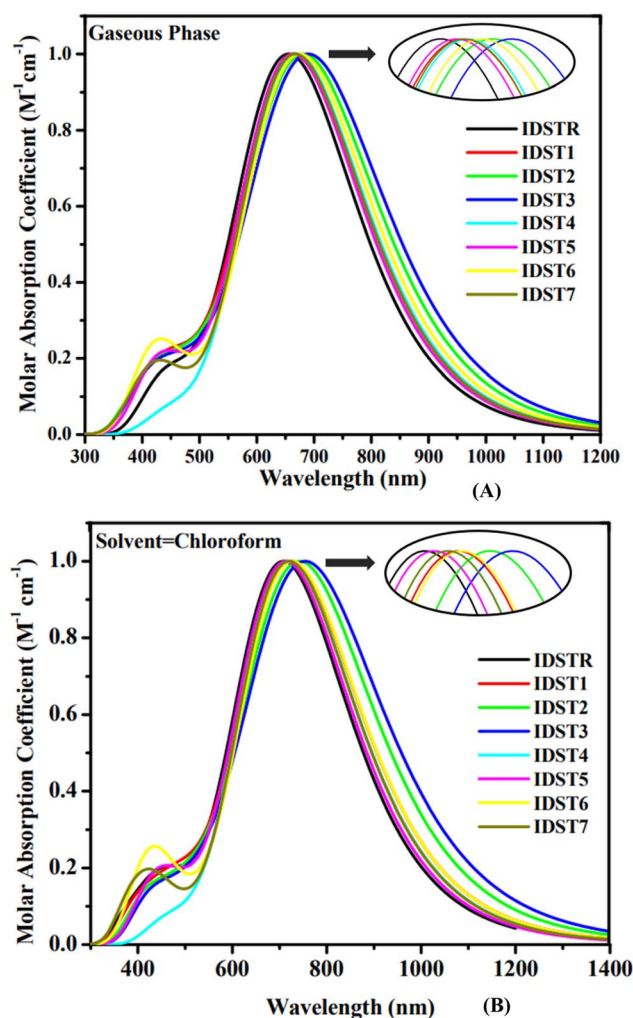

Fig. 4 Absorption spectra of IDSTR and IDST1–IDST7 in (A) gaseous phase and (B) CHCl$_3$ solvent.

shift in their $\lambda_{\max}$ in regards to the **IDSTR** molecule in both evaluated phases, with the **IDST1–IDST7** molecules exhibiting a shift of 7 nm to 42 nm and 5 nm to 58 nm, respectively. Better light absorption results from the molecules' planar structure, which promotes greater conjugation within the structure. All investigated molecules exhibited a bathochromic switch when in CHCl$_3$ solvent, as opposed to gaseous form, on the basis of the general fact that the polar solvent stabilize the polar excited state.[49] The shorter E_{gap} of all the molecules resulted in a longer wavelength due to the inverse connection of energy and wavelength.[50] The **IDSTR** and **IDST1–IDST7** molecules' rising $\lambda_{\max}$ trend in the gas phase and in the CHCl$_3$ is **IDSTR** < **IDST5** < **IDST7** < **IDST4** = **IDST1** < **IDST6** < **IDST2** < **IDST3** and **IDSTR** < **IDST5** < **IDST7** < **IDST4** < **IDST6** < **IDST1** < **IDST2** < **IDST3**, respectively. The outcomes reveal that **IDST3** has the highest $\lambda_{\max}$ in gas and solvent phases, at 701 nm and 770 nm, respectively, which may be due to the pairs of electronegative cyano group presence in the peripheral acceptor unit.

The optical properties of organic photovoltaic devices and the amount of radiation produced by electrical stimulation between two levels of energy are both highly dependent on a dimensionless quantity termed oscillator strength (f).[51] Energy needed to make a likely transition is called excitation energy (E_{x}),[52] as a matter of fact, improving ICT functionality can be achieved by expanding the absorption spectrum, decreasing the E_{x}, or raising the f.[53] Compared to **IDSTR**, **IDST1–IDST7** molecules have lower E_{x} while **IDST4–IDST7** molecules have higher f, in consequence of this, they might have more efficient ICT.

3.5. Light-harvesting efficiency (LHE)

Every component of SCs must be able to generate a charge after the absorption of light, known as LHE.[54] Short-circuit current generation is significantly affected by LHE, which than effect the device's solar efficacy.[55] Using eqn (5), the LHE of every chemical studied was computed.

$$\eta_\lambda = 1 - 10^{-f} \quad (5)$$

In above equation, η_λ is the LHE and the **IDSTR** and **IDST1–IDST7** LHE values have been computed, and they are shown in Table 6. Compared to **IDSTR**, the LHE of **IDST4–IDST7** molecules is higher because their f is higher, as LHE is directly related to f. Due to **IDST5**'s greater oscillator strength, LHE is at its ultimate level. Consistent with the findings, the LHE of

Table 6 f, and LHE of IDSTR and IDST1–IDST7

Molecules	f	LHE
IDSTR	2.58	0.9973
IDST1	2.57	0.9973
IDST2	2.51	0.9969
IDST3	2.42	0.9961
IDST4	2.79	0.9983
IDST5	2.82	0.9985
IDST6	2.80	0.9984
IDST7	2.71	0.9980

IDST5–IDST7 molecules is significantly affected by the ending acceptor moieties.

3.6. Dipole moment

The dipole moment (D) has a significant role in determining solubility as well as crystallinity. These characteristics have a crucial role in defining polarization processes in the necessary solvent for efficient organic photovoltaic devices.[56] Consistent transfer of charge is enabled by the planar and ordered morphologies of molecules with strong dipole moments, which lead to close molecular packing, improved crystallinity, as well as higher solubility in polar solvents. For better charge conduction, molecules with a larger D tend to be more crystallized and dissolve more easily in polar solvents.[42] Molecules with no dipole moment are often insoluble in polar organic solvents like chloroform. Hence the connection between them is not universal, every molecule does have a different chemical structure, which affects its charge carrier as well as solubility properties.[57] As per given numerical values in Table 7, the raising order of D for **IDSTR** and **IDST1–IDST7** molecules is same in gas phase and CHCl$_3$ solvent *i.e.*, **IDSTR** < **IDST7** < **IDST2** < **IDST6** < **IDST5** < **IDST1** < **IDST4** < **IDST3**. All modified molecules exhibit superior crystallinity and solubility than **IDSTR** due to their greater D values. The highest D value was found in **IDST3**, that may be attributed to the presence of cyano groups at both of its ends.

3.7. Charge mobility analysis

The reorganization energy (RE) of **IDST1–IDST7** and **IDSTR** molecules were determined at MPW1PW91 functional to

Table 7 Dipole moment of IDSTR and IDST1–IDST7 molecules in gas phase and CHCl$_3$ solvent

Molecules	D (gas phase)	D (solvent phase)
IDSTR	2.10	2.62
IDST1	4.66	4.83
IDST2	2.39	3.35
IDST3	11.32	13.64
IDST4	6.65	7.95
IDST5	3.74	4.54
IDST6	2.78	3.52
IDST7	2.24	2.75

Table 8 RE of electron and hole (λ_- and λ_+, respectively) for IDSTR and IDST1–IDST7 molecules

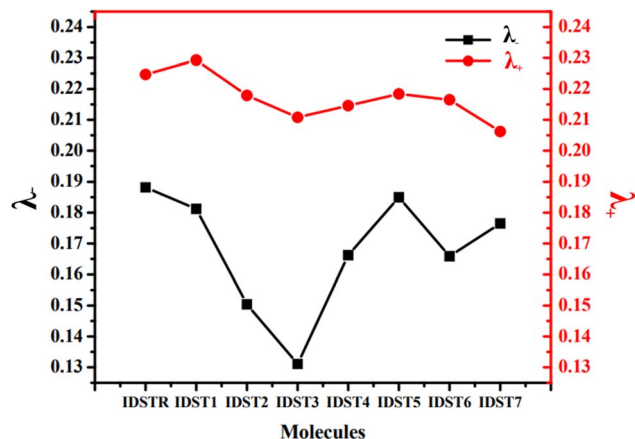| Molecules	λ_- (eV)	λ_+ (eV)
IDSTR	0.1882	0.2247
IDST1	0.1812	0.2293
IDST2	0.1504	0.2179
IDST3	0.1311	0.2108
IDST4	0.1662	0.2146
IDST5	0.1850	0.2184
IDST6	0.1659	0.2165
IDST7	0.1765	0.2062

Fig. 5 RE plot of **IDSTR** and **IDST1–IDST7** molecules.

analyze the charge transfer from donor unit acceptor unit. The main factor for the creation of effective substances for OSCs is the RE, which quantifies the charge that is transported from donor fragment to acceptor portions of a compound and is linked to the electron and hole mobility.[58] The RE has an inverse relationship to the charges mobility *i.e.*, electrons and holes. As a result, lowering the values of the RE will result in a more effective charge transport.[59] One of the many factors that affect the RE are the geometric configurations of anions and cations. RE of electron and hole are calculated for all of the investigated compounds using eqn (1) and (2), and the findings are given and shown in Table 8 and Fig. 5. The findings suggest that the improved molecular blend of planar electronic structures is responsible for the enhanced electron and hole mobilities seen in the newly suggested molecules.

The RE of the **IDSTR** molecule is 0.1882 eV for the λ_- and 0.2247 eV for the λ_+. All the modified molecules have higher electron mobilities than **IDSTR** because their RE for λ_- are smaller than those of the **IDSTR** molecule. Because of the planar molecule structure, the resulting molecular mix will have a smooth morphology, which improves exciton dissociation and electron mobility. Since the RE of **IDST3** was
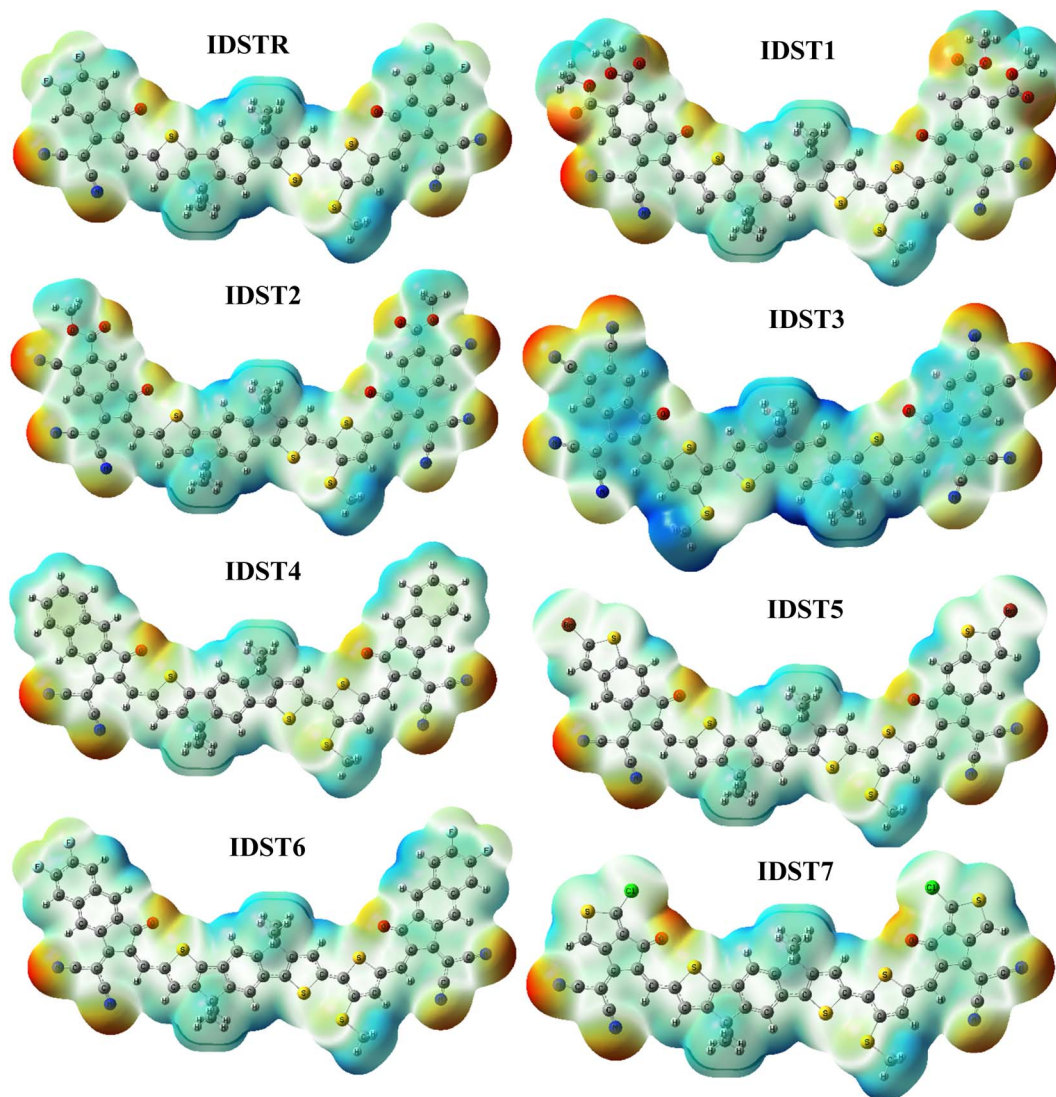

Fig. 6 ESP maps of **IDSTR** and **IDST1–IDST7** molecules.

observed to be the smallest (0.1311 eV) of all the molecules examined, this suggests that the molecule's new peripheral acceptors have had a significant impact on increasing its electron transport. The order of λ_- RE for the studied molecules is **IDST3 < IDST2 < IDST6 < IDST4 < IDST7 < IDST1 < IDST5 < IDSTR**.

IDST2–IDST7 molecules have improved mobility of hole than reference as these molecules have smaller λ_+ RE value than
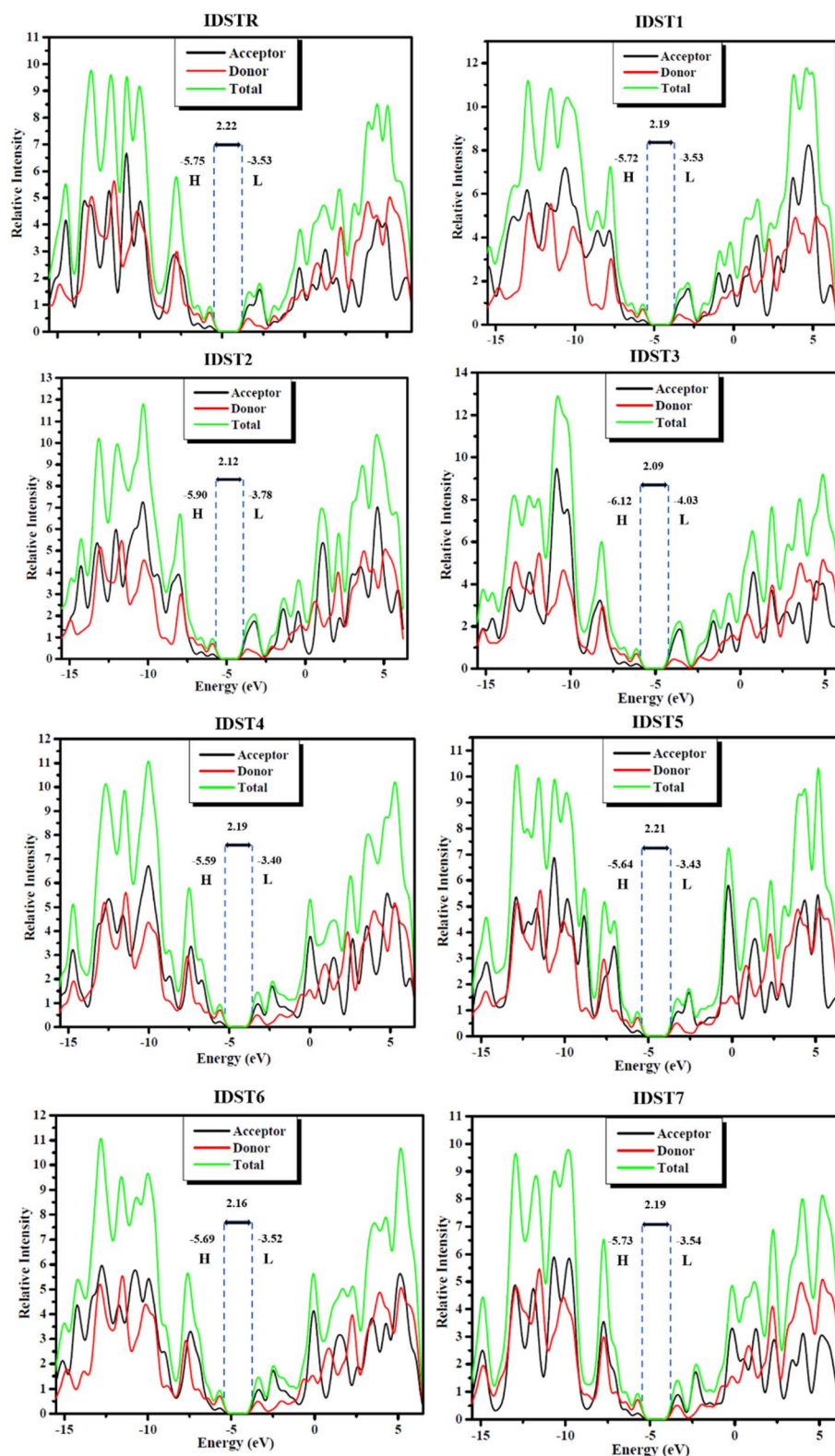

Fig. 7 DOS plots of **IDSTR** and **IDST1–IDST7** molecules.

© 2022 The Author(s). Published by the Royal Society of Chemistry

IDSTR molecule. The drastic drop in the RE of hole for the **IDST7** molecule indicates that the terminal acceptor is contributing significantly to the lowering of the RE to promote mobility of hole. **IDST7** < **IDST3** < **IDST4** < **IDST6** < **IDST2** < **IDST5** < **IDSTR** < **IDST1** is the sequence of λ_+ for the studied molecules.

3.8. Electrostatic potential (ESP)

ESP highlights the existence of electrons as well as distribution of charges on the molecule three dimensionally (3D).[60] On our carefully investigated compounds, ESP analysis was done in order to forecast the reactive sites of a molecular structure.[61] The 3D configuration of lone-pairs, electrons, and electronegative materials, which are conveniently exposed to nucleophilic activity are shown on ESP map. On the ESP mapping, red indicates an area with a high concentration of electrons, green indicates a neutral region, and blue indicates a region with a lower density of electrons.

Fig. 6 displays the **IDSTR** and **IDST1–IDST7** colorful ESP maps. An abundance of electron concentration can be seen over the oxygen as well as nitrogen atoms at the outer acceptor areas of the molecules, which shows up as dark red spots on ESP layouts.

Donor regions with thiophene rings, benzene rings and methyl groups are indicated as blue on the ESP maps, indicating an extreme deficiency of electrons at those locations.

3.9. Density of states (DOS) analysis

It is essential to carry out DOS analyses to gain a deeper comprehension of the activities of every molecule's units *i.e.*, donor, acceptor. The entire capabilities of compounds are confirmed by their corresponding DOS, which are either partial or total DOS.[61] DOS estimation is crucial in establishing the arrangement of frontier molecular orbitals (FMOs) with respect to Mulliken charge density.[62] All compounds under study had their DOS calculated by employing MPW1PW91/6-31G(d,p) level, and plots of peaks were generated in PyMOlyze 1.1. The energy (represented by the *x*-axis) and relative intensity (represented by the *y*-axis) are shown graphically in DOS plots. The HOMO energies are represented by peaks on the left of the center plane (the bandgap) in the graphs, while the LUMO energies are represented by peaks on the right. Each molecule was subdivided into its respective donor and acceptor halves for investigation of the individual unit contribution to the FMOs. In the DOS plots of **IDSTR** and **IDST1–IDST7**, donor and acceptor participation is shown by red and black lines, while overall contribution to FMO growth by the moieties is shown by a green line as seen in Fig. 7, and the participation information is included in Table 9. DOS studies showed that all compounds (**IDSTR**, **IDST1–IDST7**) had similar donor and acceptor contributions patterns, with the donor fragment being more significant in HOMO and the acceptor portions being more significant in LUMO. This clearly demonstrates the flow of charge from donor unit to acceptor units of molecule efficiently by consecutive conjugation which may increase the OSCs' ultimate efficiency. These findings corroborate with the aforementioned

Table 9 Participation of donor and acceptor units in FMOs of studied molecules

Molecules		Donor (%)	Acceptor (%)
IDSTR	HOMO	77.9	22.1
	LUMO	38.3	61.7
IDST1	HOMO	77.2	22.8
	LUMO	36.3	63.7
IDST2	HOMO	76.5	23.5
	LUMO	34.2	65.8
IDST3	HOMO	76.1	23.9
	LUMO	33.6	66.4
IDST4	HOMO	76.5	23.5
	LUMO	37.5	62.5
IDST5	HOMO	77.0	23.0
	LUMO	39.0	61.0
IDST6	HOMO	76.3	23.6
	LUMO	37.2	62.8
IDST7	HOMO	76.5	23.5
	LUMO	39.3	60.7

FMOs of **IDSTR** and **IDST1–IDST7**, as demonstrated in Fig. 3. The data show that the HOMO is dominated by the donor central part of the molecule that is rich with electrons, whereas the charge is flowing from the donor central region to the electron-withdrawing terminal units of molecules in LUMO pointing to the molecules' planar geometry, which allow for such efficient charge transfer.

3.10. Transition density matrix (TDM) and exciton binding energy (E_b)

TDM analysis is mandatory to provide an accurate forecast of exciton movement between donor and acceptor zones at specific places in conjugated molecular geometry.[63] This approach has the potential to investigate a number of different types of charge phenomena, including prediction of charge transmission, primary charge sites, and positioning of exciton movement during absorption and emission in the excited state.[64] TDM plots are usually generated to analyze electronic characteristics, such as the resonance effects and the degree of delocalization, and to get insight into the charge mobility inside a molecule. Due to the negligible impact in charge transport, hydrogen's participation is often disregarded in TDM analysis.[74,75] Numbers of atoms in compounds other than hydrogen are shown along the left *y*-axis and the lower *x*-axis, respectively. The charge density coefficient is represented by the multicolored bar on the *x*-axis of the right side, whose colors go from blue to red. As can be seen in Fig. 8, the electronic potential is existing in both the regions (acceptor and the donor) of all of the molecules we looked at (**IDSTR** and **IDST1–IDST7**). Consistency in electron density travels from donor to acceptor in a diagonal and off-diagonal pattern, with the diagonal being the more prevalent. The scheme depicted the smooth transport of electronic potential from the electron rich donor part to the acceptor component of the molecule by sequential conjugation, suggesting effective charge dispersion.
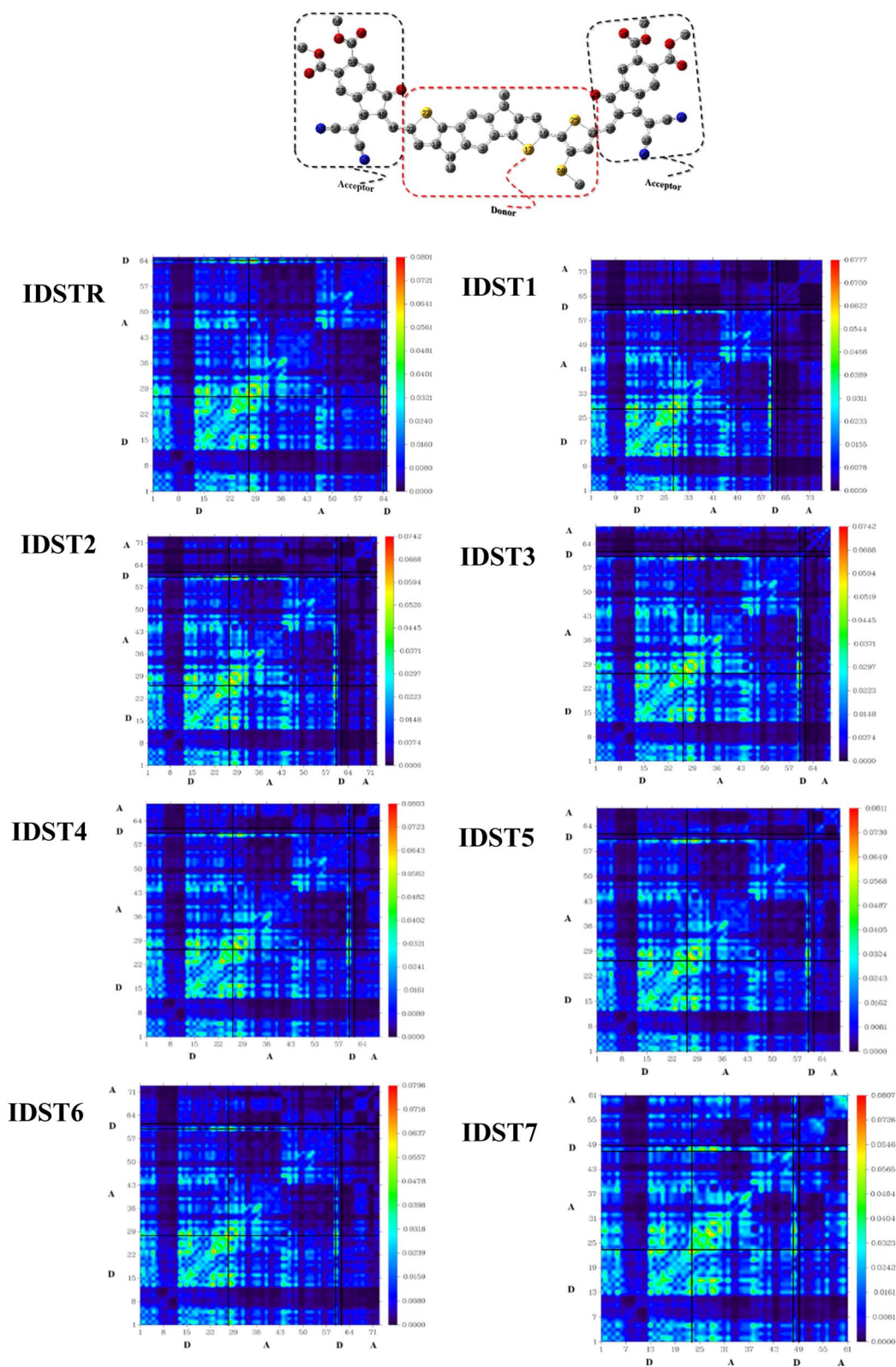
Fig. 8 TDM plots of **IDSTR** and **IDST1–IDST7** molecules.

The interaction coefficient (IC) for all studied molecules is computed and given in Table 10, as well as their increasing pattern is **IDST5** < **IDST4** < **IDST6** < **IDST1** < **IDSTR** < **IDST2** < **IDST3** < **IDST7**. The IC of **IDST5** is small which indicate that electrons can easily be transferred from the donor and acceptor sites of this molecule. This is due to the fact that increased charge mobility is predicted by a smaller IC of molecule.[57]

Table 10 E_{gap}, E_b (gas phase), E_b (CHCl$_3$ solvent), Interaction Coefficient (IC) of IDSTR and IDST1–IDST7 molecules

Molecules	E_{gap} (eV)	E_b (eV) Gaseous	E_b (eV) Solvent	IC
IDSTR	2.22	0.34	0.48	0.69670
IDST1	2.19	0.35	0.50	0.69639
IDST2	2.12	0.32	0.48	0.69673
IDST3	2.09	0.34	0.48	0.69712
IDST4	2.19	0.35	0.48	0.69591
IDST5	2.21	0.35	0.49	0.69574
IDST6	2.16	0.33	0.47	0.69619
IDST7	2.19	0.34	0.48	0.69748

The E_b is also an important consideration, that can be used to evaluate the potential for the separation of electron–hole (exciton), the performance as well as the electrical characteristics of OSCs.[65] E_b is the value that is used to calculate the

coulombic interactions that take place between electron–hole pair.[66] When the electron–hole coulombic interaction is small, as indicated by a reduced E_b, and *vice versa*. E_b was estimated using eqn (6) in this study and the results are given in Table 10.

$$E_b = E_{gap} - E_x \qquad (6)$$

The calculated values show that in the gas phase, **IDST2** and **IDST6** have the lower E_b value (at 0.32 eV and 0.36 eV respectively) compared to the **IDSTR** molecule, **IDST3** and **IDST7** are close to the reference E_b, and **IDST2** has the lowest E_b value overall. E_b of **IDST6** (0.47 eV) is smallest in CHCl$_3$ solvent. Since these molecules have lower E_b values, it is simple for exciton to diffuse into free charges, making them interesting candidates for higher charge densities.

3.11. Performance of device

An essential aspect of understanding the operation of any photovoltaic device is measuring its open circuit voltage (V_{OC}), which can done to assess its photovoltaic performance.[67] V_{OC} accurately reflects the maximum voltage that an optical device is capable of providing at zero voltage input.[68] Factors like ambient light, charge transmission, temperature of photovoltaic system, *etc.* all have a significant impact on V_{OC}.[69] The maximal voltage is achieved when the donor material's HOMO is associated to the acceptor material's LUMO. In order to achieve the increased V_{OC} values, the donor molecule must have a lower HOMO, whereas the acceptor molecule must have a greater LUMO level. A rise in V_{OC} leads to an increment in fill factor, that is the foundation for the higher PCE of solar devices. In this investigation, we coupled the HOMO of a well-known polymeric donor (PTB7-Th) with the LUMO of the recently proposed non-fullerene acceptors (**IDSTR**, **IDST1–IDST7**), to produce the maximum V_{OC} feasible. PTB7-Th, with its HOMO and LUMO of −5.20 eV and −3.60 eV respectively, is a robust donor, as shown by the existing literature. The eqn (7) was used in this study to statistically estimate V_{OC}.

$$V_{OC} = \frac{E_{acceptor}^{LUMO} - E_{donor}^{HOMO}}{e} - 0.3 \qquad (7)$$

In the preceding equation, e stands for the molecular charge, which is 1, and a factor of intersurface charge, which has a typical value of 0.30. Fig. 9 shows the theoretically predicted V_{OC} for **IDSTR** and **IDST1–IDST7** in connection with PTB7-Th,
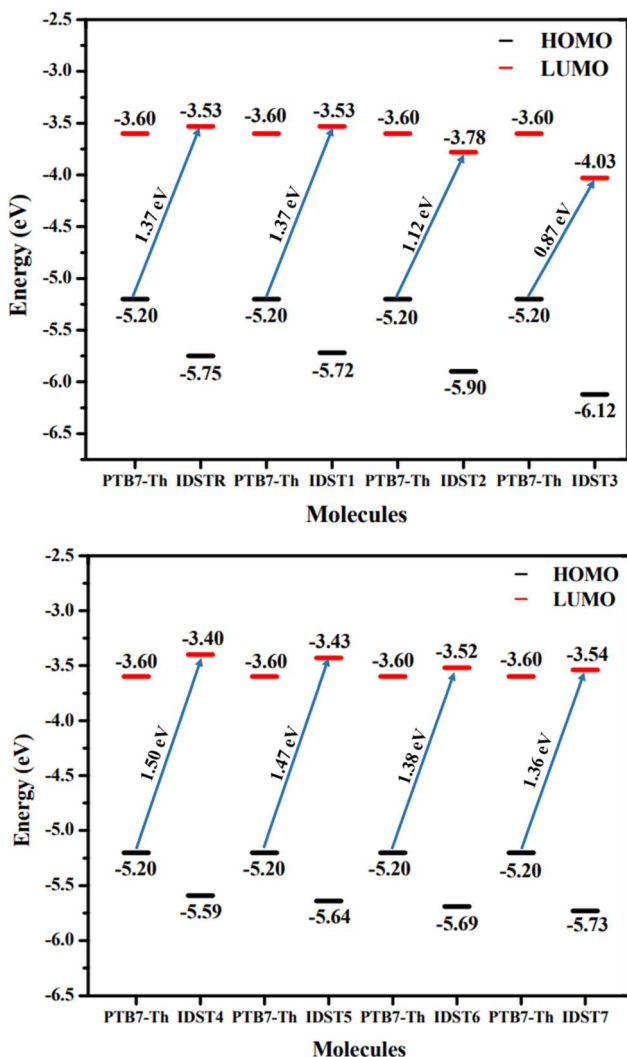
Fig. 9 Computed V_{OC} of IDSTR and IDST1–IDST7 acceptors with the combination of PTB7-Th.

Table 11 V_{OC}, normalized V_{OC} and FF of IDSTR and IDST1–IDST7

Molecule	V_{OC} (eV)	Normalized V_{OC}	FF
IDSTR	1.37	53.00	0.9077
IDST1	1.37	53.00	0.9077
IDST2	1.12	43.33	0.8920
IDST3	0.87	33.66	0.8690
IDST4	1.50	58.02	0.9140
IDST5	1.47	56.87	0.9128
IDST6	1.38	53.38	0.9082
IDST7	1.36	52.61	0.9071

and Table 11 displays the corresponding empirically predicted values. The findings show that **IDST4–IDST6** molecules have a larger V_{OC} than the **IDSTR** molecules, which have a V_{OC} of 1.37 eV. The ascending order of V_{OC} for **IDSTR** and **IDST1–IDST7** is **IDST3 < IDST2 < IDST7 < IDSTR = IDST1 < IDST6 < IDST5 < IDST4**. The **IDST4** was shown to have the greatest V_{OC} value in this study, suggesting its potential for usage in boosting OSCs' PCE.

Among the most crucial factors in calculating a PV system's PCE is its fill factor (FF), since the two are directly connected. This characteristic is significantly influenced by the V_{OC} at the donor–acceptor contact. The FF of all of our investigated compounds was calculated using eqn (8).[70]

$$FF = \frac{\frac{eV_{OC}}{K_B T} - \ln\left(\frac{eV_{OC}}{K_B T} + 0.72\right)}{\frac{eV_{OC}}{K_B T} + 1} \quad (8)$$

$\frac{eV_{OC}}{K_B T}$ is normalized V_{OC} and e is the customary charge and always equals 1. K_B is the Boltzmann constant ($8.61733034 \times 10^{-5}$ electron volts per kelvin) and T is the temperature (constant value 300 K). Table 11 displays the derived normalized V_{OC} and FF values for **IDSTR** and **IDST1–IDST7**. **IDSTR** has an FF of 0.9077 and a normalized V_{OC} of 53.00. According to the given results, **IDST4–IDST6** molecules have greater normalized V_{OC} (58.02, 56.87, 53.38) and FF (0.9140, 0.9128, 0.9082) than **IDSTR**.

The power conversion efficiency (PCE), which aggregates all solar device operational factors into a single statistic, is estimated to determine if the solar substance is sufficiently efficient for usage in operational implementations.[71] The PCE of a molecule is affected in a direct manner by the V_{OC}, FF, and the short circuit voltage (J_{SC}). This connection is well described by eqn (9).[72]

$$PCE = \frac{J_{SC} V_{OC} FF}{P_{in}} \quad (9)$$

In this work, we hypothetically determine the V_{OC} and FF using the previous equation for the **IDSTR** and **IDST1–IDST7** molecules; however, the J_{SC} has not been computed because of the inadequate facilities associated. The LHE, which is one of the J_{SC}'s criteria, has already been analyzed above. Based on the above findings, the PCE of **IDST1** and **IDST7** molecules is predicted to be very close to that of **IDSTR**. **IDST4**, **IDST5**, and **IDST6** molecules have a greater PCE since they have a higher LHE, V_{OC} and FF than **IDSTR**. The theoretical estimations demonstrate that these non-fullerene acceptors may be useful in practice due to their outstanding optoelectronic characteristics.

4 Conclusion

In this computational approach, seven new indaceno dithiophene based small acceptor molecules (**IDST1–IDST7**) have been developed of A–D–A type by the alteration of **IDSTR**

molecule. A variety of optoelectronic aspects such as energy levels of HOMO–LUMO with E_{gap}, optical bandgap, EA and IP, transition density matrix, LHE, oscillator strength, absorbance maxima (λ_{max}), binding energy, density of states, RE for the mobility of hole and electron, V_{OC} of **IDSTR** and **IDST1–IDST7** molecules have been investigated in this research by employing MPW1PW91 functional and 6-31G(d,p) basis set. The outcomes revealed that newly altered molecules (**IDST1–IDST7**) have reduced E_{gap}, higher λ_{max} as well as smaller excitation energy than **IDSTR** molecule. According to the estimations, **IDST3** possesses the shortest E_{gap} (2.09 eV) lowest E_x (1.61 eV), as well as greatest λ_{max} (770 nm). LHE of **IDST4–IDST7** is more efficient than **IDSTR** and among all **IDST5** has the maximum LHE (0.9985) due to its highest oscillator strength (2.82). All modified molecules exhibit superior crystallinity and solubility due to their greater dipole moment values (2.75–13.64 D) than the dipole moment of **IDSTR** (2.62 D). **IDST1–IDST7** molecules have higher electron mobilities than **IDSTR** because their RE for λ_- (0.1311–0.1812 eV) are smaller than those of the **IDSTR** (0.1882 eV) molecule. **IDST2–IDST7** molecules have improved mobility of hole than reference as these molecules have smaller λ_+ RE (0.2061–0.2184 eV) value than **IDSTR** molecule (0.2247 eV). By coupling the **IDST1–IDST7** acceptors with PTB7-Th donor the V_{OC} was estimated and the results showed that V_{OC} of **IDST4** (1.50 eV), **IDST5** (1.47 eV) and **IDST6** (1.38 eV) is higher than **IDSTR** V_{OC} (1.37 eV). These results suggest that **IDST4**, **IDST5**, and **IDST6** are the most promising choices for using these altered molecules in the potential development of OSCs with improved photovoltaic properties.

Author contributions

Conflicts of interest

The authors of this manuscript proclaim no conflicts of interest.

Acknowledgements

References

1 G. Zhang, J. Zhao, P. C. Chow, K. Jiang, J. Zhang, Z. Zhu, J. Zhang, F. Huang and H. Yan, *Chem. Rev.*, 2018, **118**, 3447–3507.

2 G. Wang, M. A. Adil, J. Zhang and Z. Wei, *Adv. Mater.*, 2019, **31**, 1805089.

3 H. Wang, J. Cao, J. Yu, Z. Zhang, R. Geng, L. Yang and W. Tang, *J. Mater. Chem. A*, 2019, **7**, 4313–4333.

4 Y. Huang, E. J. Kramer, A. J. Heeger and G. C. Bazan, *Chem. Rev.*, 2014, **114**, 7006–7043.

5 Y. He, H.-Y. Chen, J. Hou and Y. Li, *J. Am. Chem. Soc.*, 2010, **132**, 1377–1382.

6 M. Reyes-Reyes, K. Kim, J. Dewald, R. López-Sandoval, A. Avadhanula, S. Curran and D. L. Carroll, *Org. Lett.*, 2005, **7**, 5749–5752.

7 B. A. Collins, J. R. Tumbleston and H. Ade, *J. Phys. Chem. Lett.*, 2011, **2**, 3135–3145.

8 C. Yan, S. Barlow, Z. Wang, H. Yan, A. K.-Y. Jen, S. R. Marder and X. Zhan, *Nat. Rev. Mater.*, 2018, **3**, 1–19.

9 H. Chen, Y. Zou, H. Liang, T. He, X. Xu, Y. Zhang, Z. Ma, J. Wang, M. Zhang and Q. Li, *Sci. China: Chem.*, 2022, 1–12.

10 J. Zhang, H. S. Tan, X. Guo, A. Facchetti and H. Yan, *Nat. Energy*, 2018, **3**, 720–731.

11 X. Wang, H. Chen, A.-R. Ran, L. Luo, P. P. Chan, C. C. Tham, R. T. Chang, S. S. Mannil, C. Y. Cheung and P.-A. Heng, *Med. Image Anal.*, 2020, **63**, 101695.

12 T. Liu, R. Ma, Z. Luo, Y. Guo, G. Zhang, Y. Xiao, T. Yang, Y. Chen, G. Li and Y. Yi, *Energy Environ. Sci.*, 2020, **13**, 2115–2123.

13 L. Zhan, S. Li, T.-K. Lau, Y. Cui, X. Lu, M. Shi, C.-Z. Li, H. Li, J. Hou and H. Chen, *Energy Environ. Sci.*, 2020, **13**, 635–645.

14 F. Huang, T. He, M. Li, L. Meng, W. Feng, H. Liang, Y. Zhou, X. Wan, C. Li and G. Long, *Chem. Mater.*, 2022, **34**, 6009–6025.

15 C. Yan, S. Barlow, Z. Wang, H. Yan, A. K. Y. Jen, S. R. Marder and X. Zhan, *Nat. Rev. Mater.*, 2018, **3**, 18003.

16 T. Li, S. Dai, Z. Ke, L. Yang, J. Wang, C. Yan, W. Ma and X. Zhan, *Adv. Mater.*, 2018, **30**, 1705969.

17 J. Zhu, Z. Ke, Q. Zhang, J. Wang, S. Dai, Y. Wu, Y. Xu, Y. Lin, W. Ma and W. You, *Adv. Mater.*, 2018, **30**, 1704713.

18 S. Dai, T. Li, W. Wang, Y. Xiao, T. K. Lau, Z. Li, K. Liu, X. Lu and X. Zhan, *Adv. Mater.*, 2018, **30**, 1706571.

19 S. Dai, Y. Xiao, P. Xue, J. James Rech, K. Liu, Z. Li, X. Lu, W. You and X. Zhan, *Chem. Mater.*, 2018, **30**, 5390–5396.

20 Y. Liu, Z. Zhang, S. Feng, M. Li, L. Wu, R. Hou, X. Xu, X. Chen and Z. Bo, *J. Am. Chem. Soc.*, 2017, **139**, 3356–3359.

21 J. Lee, S. J. Ko, M. Seifrid, H. Lee, C. McDowell, B. R. Luginbuhl, A. Karki, K. Cho, T. Q. Nguyen and G. C. Bazan, *Adv. Energy Mater.*, 2018, **8**, 1801209.

22 S. Feng, C. e. Zhang, Y. Liu, Z. Bi, Z. Zhang, X. Xu, W. Ma and Z. Bo, *Adv. Mater.*, 2017, **29**, 1703527.

23 S. Li, L. Zhan, N. Yao, X. Xia, Z. Chen, W. Yang, C. He, L. Zuo, M. Shi and H. Zhu, *Nat. Commun.*, 2021, **12**, 1–11.

24 D. Liu, Q. Zhu, C. Gu, J. Wang, M. Qiu, W. Chen, X. Bao, M. Sun and R. Yang, *Adv. Mater.*, 2016, **28**, 8490–8498.

25 Q. Guo, J. Lin, H. Liu, X. Dong, X. Guo, L. Ye, Z. Ma, Z. Tang, H. Ade and M. Zhang, *Nano Energy*, 2020, **74**, 104861.

26 J. Lin, Q. Guo, Q. Liu, J. Lv, H. Liang, Y. Wang, L. Zhu, F. Liu, X. Guo and M. Zhang, *Chin. J. Chem.*, 2021, **39**, 2685–2691.

27 A. Frisch, *Gaussian 09W Reference*, Wallingford, USA, 2009, p. 25.

28 M. Frisch, G. Trucks, H. Schlegel, G. Scuseria, M. Robb, J. Cheeseman, G. Scalmani, V. Barone, B. Mennucci and G. Petersson, 2009, see also: https://gaussian.com/.

29 B. Civalleri, C. M. Zicovich-Wilson, L. Valenzano and P. Ugliengo, *CrystEngComm*, 2008, **10**, 405–410.

30 T. Yanai, D. P. Tew and N. C. Handy, *Chem. Phys. Lett.*, 2004, **393**, 51–57.

31 C. Adamo and V. Barone, *J. Chem. Phys.*, 1998, **108**, 664–675.

32 J.-D. Chai and M. Head-Gordon, *Phys. Chem. Chem. Phys.*, 2008, **10**, 6615–6620.

33 M. D. Hack and D. G. Truhlar, *J. Phys. Chem. A*, 2000, **104**, 7917–7926.

34 J. Tomasi, B. Mennucci and R. Cammi, *Chem. Rev.*, 2005, **105**, 2999–3094.

35 L. Deschenes and A. David, https://www.originlab.com, Commercial price, 2000, vol. 595.

36 T. Lu and F. Chen, *J. Comput. Chem.*, 2012, **33**, 580–592.

37 A. Tenderholt, Stanford University, CA Stanford, 2006.

38 S. Alexander and R. Orbach, *J. Phys., Lett.*, 1982, **43**, 625–631.

39 Z. Shuai, W. Li, J. Ren, Y. Jiang and H. Geng, *J. Chem. Phys.*, 2020, **153**, 080902.

40 E. U. Rashid, J. Iqbal, M. I. Khan, Y. A. El-Badry, K. Ayub and R. A. Khera, *RSC Adv.*, 2022, **12**, 12321–12334.

41 G. R. Hutchison, M. A. Ratner and T. J. Marks, *J. Am. Chem. Soc.*, 2005, **127**, 2339–2350.

42 M. I. Khan, J. Iqbal, S. J. Akram, Y. A. El-Badry, M. Yaseen and R. A. Khera, *J. Mol. Graphics Modell.*, 2022, **113**, 108162.

43 J. Zhou, X. Wan, Y. Liu, G. Long, F. Wang, Z. Li, Y. Zuo, C. Li and Y. Chen, *Chem. Mater.*, 2011, **23**, 4666–4668.

44 E. U. Rashid, J. Iqbal, R. F. Mehmood, Y. A. El-Badry, S. J. Akram and R. A. Khera, *Comput. Theor. Chem.*, 2022, **1211**, 113669.

45 E. U. Rashid, N. Hadia, J. Iqbal, R. F. Mehmood, H. Somaily, S. J. Akram, A. M. Shawky, M. I. Khan, S. Noor and R. A. Khera, *RSC Adv.*, 2022, **12**, 21801–21820.

46 J. Widmer, M. Tietze, K. Leo and M. Riede, *Adv. Funct. Mater.*, 2013, **23**, 5814–5821.

47 A. Farhat, R. A. Khera, S. Iqbal and J. Iqbal, *Opt. Mater.*, 2020, **107**, 110154.

48 H. Sahu and A. N. Panda, *Phys. Chem. Chem. Phys.*, 2014, **16**, 8563–8574.

49 U. Azeem, R. A. Khera, A. Naveed, M. Imran, M. A. Assiri, M. Khalid and J. Iqbal, *ACS Omega*, 2021, **6**, 28923–28935.

50 Y. Tian, K. Wang, H. Zhang, X. Wu and C. Zhong, *Tetrahedron*, 2022, **113**, 132756.

51 I. Zubair, R. A. Kher, S. J. Akram, Y. A. El-Badry, M. U. Saeed and J. Iqbal, *Chem. Phys. Lett.*, 2022, **793**, 139459.

52 M. U. Saeed, J. Iqbal, R. F. Mehmood, M. Riaz, S. J. Akram, H. Somaily, A. M. Shawky, M. Raheel, M. I. Khan and E. U. Rashid, *J. Phys. Chem. Solids*, 2022, 110906.

53 M. Waqas, J. Iqbal, R. F. Mehmood, S. J. Akram, A. M. Shawky, M. Raheel, E. U. Rashid and R. A. Khera, *J. Mol. Graphics Modell.*, 2022, **116**, 108255.

54 M. Rafiq, R. A. Khera, M. Salim, M. Khalid, K. Ayub and J. Iqbal, *Chem. Phys. Lett.*, 2021, **782**, 139018.

55 M. U. Saeed, J. Iqbal, R. F. Mehmood, S. J. Akram, Y. A. El-Badry, S. Noor and R. A. Khera, *Surf. Interfaces*, 2022, **30**, 101875.

56 A. Sharif, S. Jabeen, S. Iqbal and J. Iqbal, *Mater. Sci. Semicond. Process.*, 2021, **127**, 105689.

57 M. Rafiq, M. Salim, S. Noreen, R. A. Khera, S. Noor, U. Yaqoob and J. Iqbal, *J. Mol. Liq.*, 2022, **345**, 118138.

58 M. R. Aslam, R. A. Khera, Y. A. El-Badry, M. Rafiq, A. Naveed, M. T. Shehzad and J. Iqbal, *J. Mol. Graphics Modell.*, 2022, **112**, 108146.

59 N. E. Gruhn, D. A. da Silva Filho, T. G. Bill, M. Malagoli, V. Coropceanu, A. Kahn and J.-L. Brédas, *J. Am. Chem. Soc.*, 2002, **124**, 7918–7919.

60 H. Yao, Y. Cui, D. Qian, C. S. Ponseca Jr, A. Honarfar, Y. Xu, J. Xin, Z. Chen, L. Hong and B. Gao, *J. Am. Chem. Soc.*, 2019, **141**, 7743–7750.

61 M. Ans, J. Iqbal, B. Eliasson and K. Ayub, *Comput. Mater. Sci.*, 2019, **159**, 150–159.

62 C. Fonseca Guerra, J. W. Handgraaf, E. J. Baerends and F. M. Bickelhaupt, *J. Comput. Chem.*, 2004, **25**, 189–210.

63 P. Å. Malmqvist, *Int. J. Quantum Chem.*, 1986, **30**, 479–494.

64 A. Luzanov, A. Sukhorukov and V. Umanskii, *Theor. Exp. Chem.*, 1976, **10**, 354–361.

65 P. Gong, P. Guo, Y. Wang, L. Yan, Z. Liang, M. Ding, J. Tong, J. Li and Y. Xia, *ACS Appl. Energy Mater.*, 2021, **4**, 9627–9638.

66 Y. A. Duan, Y. Geng, H. B. Li, J. L. Jin, Y. Wu and Z. M. Su, *J. Comput. Chem.*, 2013, **34**, 1611–1619.

67 U. Mubashar, A. Farhat, R. A. Khera, N. Iqbal, R. Saleem and J. Iqbal, *J. Mol. Model.*, 2021, **27**, 1–13.

68 M. Salim, M. Rafiq, R. A. Khera, M. Arshad and J. Iqbal, *Sol. Energy*, 2022, **233**, 31–45.

69 I. Zubair, R. A. Khera, A. Naveed, R. A. Shehzad and J. Iqbal, *Mater. Sci. Semicond. Process.*, 2022, **148**, 106812.

70 J. D. Chen, C. Cui, Y. Q. Li, L. Zhou, Q. D. Ou, C. Li, Y. Li and J. X. Tang, *Adv. Mater.*, 2015, **27**, 1035–1041.

71 R. Rajeswari, N. Islavath, M. Raghavender and L. Giribabu, *Chem. Rec.*, 2020, **20**, 65–88.

72 H. Yao, L. Ye, H. Zhang, S. Li, S. Zhang and J. Hou, *Chem. Rev.*, 2016, **116**, 7397–7457.

73 M. Ans, F. Manzoor, K. Ayub, F. Nawaz and J. Iqbal, *J. Mol. Model.*, 2019, **25**, 1–12.

74 M. Ans, M. Paramasivam, K. Ayub, R. Ludwig, M. Zahid, X. Xiao and J. Iqbal, *J. Mol. Liq.*, 2020, **305**, 112829.

75 M. Ans, K. Ayub, S. Muhammad and J. Iqbal, *Comput. Theor. Chem.*, 2019, **1161**, 26–38.